Published in final edited form as:
Biochemistry. 2010 December 21; 49(50): 10595–10605. doi:10.1021/bi101394r.

Limiting an Antimicrobial Peptide to the Lipid-Water Interface Enhances its Bacterial Membrane Selectivity – A Case Study on MSI-367

Sathiah Thennarasu[1,2], **Rui Huang**[2], **Dong-Kuk Lee**[1,2], **Pei Yang**[1], **Lee Maloy**[3], **Zhan Chen**[1,2], and **Ayyalusamy Ramamoorthy**[1,2,*]

[1] Department of Biophysics, University of Michigan, Ann Arbor, MI 48109-1055

[2] Department of Chemistry, University of Michigan, Ann Arbor, MI 48109-1055

[3] Genaera Pharmaceuticals, Plymouth Meeting, PA 19462

Abstract

In a minimalist design approach, a synthetic peptide MSI-367 [$(KFAKKFA)_3$-NH_2)] was designed and synthesized with an objective towards generating cell-selective non-lytic peptides, which have a significant bearing in cell-targeting. The peptide showed potent activity against both bacteria and fungi, but no toxicity to human cells at micromolar concentrations. Bacterial versus human cell membrane selectivity of the peptide was determined from membrane permeabilization assays. Circular dichroism investigations revealed the intrinsic helix propensity of the peptide, β-turn structure in aqueous buffer and, extended and turn conformations upon binding to lipid vesicles. DSC experiments on DiPOPE bilayers indicated the induction of positive curvature strain and repression of fluid lamellar to inverted hexagonal phase transition by MSI-367. Results from ITC experiments suggested the possibility of formation of specific lipid-peptide complexes leading to aggregation. ^{2}H NMR of deuterated-POPC multilamellar vesicles confirmed the limited effect of membrane embedded peptide at the lipid-water interface. ^{31}P NMR data indicated changes in the lipid head group orientation of POPC, POPG, and POPE lipid bilayers upon peptide binding. Membrane-embedded and membrane-inserted states of the peptide were observed in sum frequency generation vibrational spectroscopy. CD, ITC and ^{31}P NMR data on *E. coli* lipids agree with the hypothesis that strong electrostatic lipid-peptide interactions embrace the peptide at the lipid-water interface and provide the basis for bacterial cell selectivity.

Keywords

antimicrobial peptide; bacterial selectivity; membrane adsorption; solid-state NMR

Antimicrobial peptides (AMPs) are produced as a part of host defense mechanisms by various organisms that include microbes, insects, plants, vertebrates and mammals (1–5). Most of the antimicrobial peptides are hydrophobic and cationic, and exert their activity against pathogens by interacting with target cell membranes (6–8). An intriguing aspect of AMPs is that these peptides are not toxic to the epithelial and immune cells of host organism but only disrupt the membrane of microbes and pathogens. The remarkable ability of AMPs to selectively disrupt the membrane of pathogens has been documented (9–18). However, the exact attributes for target cell membrane selectivity are not clearly understood, partly

*Author to whom correspondence should be addressed Correspondence: Ayyalusamy Ramamoorthy, Phone: (734) 647-6572, FAX: (734) 764-3323, ramamoor@umich.edu.

because of the variance in primary structure of AMPs and environment dependent propensity to adopt secondary conformations.

The membrane activity of linear antimicrobial peptides is generally explained in terms of three distinct steps: (1) an unstructured, or partially structured monomeric state in water, (2) membrane embedded partially structured monomeric, or oligomeric state, and (3) inserted across the lipid bilayer as a monomer or bundle. Amphipathic α-helical peptides that exhibit both antimicrobial and hemolytic activities have been demonstrated to insert across the lipid bilayer (19–23). A subset of AMPs, especially the short peptides, has been reported to exert only antimicrobial activity and low or negligible hemolytic activity without causing substantial membrane disruption (24–30). Structurally constrained cyclic peptides also display selective adsorption to bacterial membranes (31–33). Peptide toxins and designer cell-lytic peptides are known to display both antimicrobial and hemolytic properties, and insert across the lipid bilayer (34–37). A significant number of designer peptides have been developed to improve upon the therapeutic potential of AMPs in general (37–41). However, toxicity to human cells remains a major concern in the development of therapeutic peptide antibiotics. In the context of AMP related toxicity, we hypothesize that hemolytic activity can be averted selectively by limiting the peptide-membrane interactions at the lipid-water interface and thereby preventing peptide insertion and membrane lysis.

In this study, we tested our hypothesis using a 21-residue synthetic antimicrobial peptide MSI-367, composed of only three amino acid residues. In this report, we provide evidence for selective permeabilization of a bacterial membrane over a red blood cell membrane. We show the surface binding of the peptide from the lipid order parameters derived from ^{31}P and de-Paked ^{2}H-NMR spectra of peptide-incorporated lipid bilayers. Using ^{31}P-NMR of mechanically oriented lipid bilayers, we demonstrate the lipid selective interactions of the peptide. We show the membrane embedded conformation of the peptide using circular dichroism (CD) measurements. We also show the effect of membrane bound peptide on the phase transition (T_H) behavior of lipid vesicles. In addition, we present the enthalpy changes associated with peptide-induced changes in zwitterionic and acidic lipid vesicles. Moreover, we deduce the orientation of membrane bound peptide axis using sum frequency generation (SFG) vibrational spectroscopy. Further, the ramifications of this study are discussed in terms of bacterial cell selective activity stemming from the formation of specific peptide-lipid complexes.

Materials and Methods

Materials

All lipids were purchased from Avanti Polar Lipids (Alabaster, AL). Chloroform and methanol were procured from Aldrich Chemical Inc. (Milwaukee, WI). Naphthalene was from Fisher Scientific (Pittsburgh, PA). Buffers were prepared using water obtained from NANOpure A filtration system. All solvents and reagents were purchased from Bachem, Synthetech Inc., Aldrich Chemical Co., Fisher Scientific and Protein Technologies. All chemicals were used without further purification. Peptides MSI-78 and MSI-367 were synthesized using standard Fmoc-chemistry protocols by Genaera Corporation (Plymouth Meeting, PA).

Antimicrobial assay

A doubling dilution series of peptide, beginning with 100 μg/mL, was added to the wells of a sterile 384-well microtiter plate (12 replicates per dilution) and dried overnight in a desiccator box. Bacterial suspensions (10 μL, 10^7/mL) were added to the wells, covered with a sterile plastic film, centrifuged briefly to collect the cells in the bottom of the wells,

and incubated at 37°C for 6–36 hours, depending upon the rate of growth of the bacterial species. Bacteria were incubated in normal atmosphere. The terminal cell numbers were determined by turbidometric method (OD_{600} = 0.02). MICs were set as the lowest concentration of the peptide at which there was no growth above the inoculated level of bacteria ($p < 0.05$, n = 12). Values expressed in Table 1 represent Log_{10} growth above inoculated levels.

Hemolysis assay

The hemolytic activity of the peptides was determined by measuring the hemoglobin released from suspensions of fresh sheep erythrocytes. Red blood cells (Colorado Serum Co., Denver, CO) were centrifuged and washed three times with phosphate-buffered saline (0.15 M NaCl, 0.05 M phosphate buffer, pH 7.4). One hundred microliters of red blood cells was added to the wells of a 96-well plate, and then 100 μL of the peptide solution [in PBS (phosphate-buffered saline)] was added to each well. The plates were covered with an adhesive plastic sheet, incubated for 1 h at 37 °C, and centrifuged at 200*g* for 10 min. Absorbance of the supernatants was measured at 414 nm. Zero and hundred percent hemolysis was determined in PBS and 0.1% Triton X-100, respectively.

Outer-membrane disruption Assay

The outer-membrane permeabilizing ability was investigated using the 1-anilinonaphthalene-8-sulfonic acid (ANS) uptake assay (41), on *E. coli* strain BL21 (DE3). Bacterial cells from an overnight culture were inoculated into LB medium. Cells from the mid-log phase were centrifuged and washed with PBS buffer (10 mM phosphate, 150 mM NaCl, pH 7.4), and then resuspended in PBS buffer to an OD_{600} of 1.2. To 3.0 mL of the cell suspension in a cuvette, a stock solution of ANS was added to a final concentration of 5.0 μM. The degree of membrane disruption as a function of peptide concentration was observed by the increase in fluorescence intensity at ~500 nm.

Circular dichroism

Small unilamellar vesicles (SUVs) were prepared by sonication. Different lipids in appropriate proportions were dissolved in chloroform and the clear solution was taken to dryness. PBS buffer (10 mM sodium phosphate, 150 mM NaCl, 2 mM EDTA, pH 7.4) was added to dry lipid film and subjected to vortex and sonication to obtain a clear dispersion of SUVs. CD spectra were recorded (JASCO Spectropolarimeter, Model: J-715-150S) at 25 °C using samples with a peptide/lipid ratios ~1:100 and ~1:200 in a quartz cuvette (path length = 0.1 cm) over the range from 190 to 250 nm. Contributions from the buffer and SUVs were removed by subtracting the spectra of the corresponding control samples without peptide. The resultant spectra were normalized for path length and concentration. An aliquot of peptide stock solution was added using a Hamilton syringe to preformed SUVs suspended in PBS buffer and incubated at room temperature for ~5 min to allow equilibrium binding before recording CD spectra. The peptide concentration was 74.5 μg/mL.

Solid-state NMR

Mechanically-aligned POPC, POPE, POPG and *E. coli* total lipid bilayers were prepared using the procedure described elsewhere (42). Briefly, 4 mg of lipid and an appropriate amount of peptide were dissolved in $CHCl_3/CH_3OH$ (2:1) mixture. The sample was dried under a stream of nitrogen and dissolved in $CHCl_3/CH_3OH$ (2:1) mixture containing equimolar quantities of naphthalene. An aliquot of the solution (~300 μL) was spread on two thin glass plates (11 mm × 22 mm × 50 μm, Paul Marienfeld GmbH & Co., Bad Mergentheim, Germany). The samples were air-dried and then kept under vacuum for at least 10 hours at 37 °C to remove naphthalene and any residual organic solvents. After

drying, the samples were hydrated at 93% relative humidity using saturated $NH_4H_2PO_4$ solution for 2–3 days at 37 °C, after which approximately 2 μL of H_2O was misted onto the surface of the lipid-peptide film to increase the water content and therefore the extent of hydration of lipid bilayers in the sample. The glass plates were stacked, wrapped with parafilm, sealed in plastic bags (Plastic Bagmart, Marietta, GA), and then kept at 4 °C for 6–24 hours.

^{31}P-NMR spectra of mechanically-aligned lipid bilayers were obtained from a Varian Infinity 400 MHz solid-state NMR spectrometer operating at a resonance frequency of 161.979 MHz for ^{31}P nucleus. A Chemagnetics temperature controller was used to maintain the sample temperature, and each sample was equilibrated at 30 °C for at least 30 minutes before the experiment was started. The lipid bilayers were positioned in such a way that the bilayer-normal was parallel to the external magnetic field axis. A home-built double-resonance probe, which has a four-turn square-coil (12 mm × 12 mm × 4 mm) constructed using a 2 mm wide flat-wire and a spacing of 1 mm between turns, was used. A typical ^{31}P 90°-pulse length of 3.1 μs was used. ^{31}P NMR spectra were obtained using a spin-echo sequence (90°-τ-180° with τ = 100 μs), 30 kHz proton-decoupling RF field, 50 kHz spectral width, and a recycle delay of 3 seconds. A typical spectrum required the co-addition of 100–1000 transients. The ^{31}P chemical shift spectra are referenced relative to 85% H_3PO_4 on thin glass plates (0 ppm). Data processing was accomplished using the software Spinsight (Chemagnetics/Varian) on a Sun Sparc workstation.

Differential scanning calorimetry

Both peptide and DiPoPE were dissolved in $CHCl_3$/CH_3OH (2:1) mixture. The solution was dried under a stream of nitrogen and then under high vacuum for several hours. Buffer (10 mM Tris-HCl, 100 mM NaCl, 2 mM EDTA, pH 7.4) was added to each sample and vortexed to resuspend the peptide and lipid. The final concentration was 10 mg/ml lipid solution. The solutions were degassed under vacuum for 15 min before DSC measurements. The heating scan rate was 1°C/min. The L_α-to-H_{II} transition temperature of lipids was measured on a CSC 6100 Nano II Differential Scanning Calorimeter (Calorimetry Sciences, Provo, UT). The raw data were then converted to molar heat capacity using the CPCalc program available with the calorimeter. In each conversion, the average lipid molecular weight for each sample and a partial specific volume of 0.956 mL/g were used.

Isothermal titration calorimetry

The enthalpy of lipid-peptide mixing reaction was measured using a high sensitivity isothermal titration calorimeter (TA Instruments, Nano ITC 2G). Peptide and lipid solutions in PBS buffer were degassed under vacuum prior to use. The calorimeter was calibrated as recommended by the manufacturer. The heats of dilution for successive 10 μL injections of the lipid suspension (~7.2 mM) into PBS buffer (pH 7.4) were insignificant compared to the heats of peptide-lipid reaction. The peptide concentration was 5 μM. The heat liberated from successive injection of lipid was determined by integrating the area under each titration curve using the built-in NanoAnalyze software.

Sum frequency generation experiments

The Sum Frequency Generation (SFG) spectrometer setup used in this study was purchased from EKSPLA. Langmuir-Blodgett and Langmuir-Schaefer (LB/LS) methods were used to deposit the proximal and the distal leaflets of POPG, respectively. Langmuir-Blodgett and Langmuir-Schaefer (LB/LS) methods (43) were used to deposit the proximal and the distal leaflets of POPG, respectively (44). A CaF_2 prism was attached to a sample holder and the right-angle face was perpendicularly immersed in the water inside Langmuir trough. An appropriate amount of lipid-chloroform solution was then gently spread onto the water

surface, and chloroform was allowed to evaporate. The lipid monolayer area was compressed by two barriers at a rate of 5 mm/min until a surface pressure of 34 mN/m was reached. The prism was lifted out of the subphase at a rate of 1 mm/min to obtain a monolayer of lipid on the prism. The right-angle surface of the prism with the monolayer was horizontally lowered to contact again the monolayer deposited on the water surface (with a surface pressure of 34 mN/m) of the trough to form a lipid bilayer. After the formation of the bilayer, the extra lipids at the air-water interface were removed using a micropipet. The bilayer was immersed in water kept in a 2.0 mL reservoir. For peptide-bilayer interaction experiments, a specific volume of the aqueous stock solution of MSI-367 or MSI-78 was injected into the 2.0 mL reservoir to achieve the desired concentration of the peptide. A magnetic microstirrer was used to ensure a homogeneous reservoir concentration. All experiments were carried out at room temperature (~24 °C). SFG amide I spectra were collected from the peptides associated with the lipid bilayer using *ssp* (*s*-polarized sum frequency signal beam, *s*-visible input beam, and *p*-IR input beam) and *ppp* polarization combinations.

Results

Design of a cationic, amphipathic, linear MSI-367

Since a minimum of 21-residues in the α-helical conformation are required to span the membrane bilayer (45), MSI-367 was designed using three repeat units of a weakly membrane active heptapeptide (KFAKKFA) represented by only three amino acids. The hydrophobicity values of Lys, Ala and Phe (are −3.9, 1.8 and 2.8, respectively) are effectively utilized in the designing a membrane-interface seeking peptide like MSI-367 with a low aliphatic index (46,47). With a predicted ~48% helical propensity index (48) the peptide MSI-367 can be expected to fold into a maximum of five helical turns under favorable conditions. The peptide has 9 positively charged lysine residues, and therefore can, preferentially and simultaneously, bind to 9 negatively charged lipids in membranes such as bacterial and tumor cell membranes. Since alanine is weakly hydrophobic and aromatic residues have a tendency to seek membrane-water interface, six alanine and six phenylalanine residues were judiciously incorporated to limit the association of the peptide at the lipid-water interface. The overall aliphatic index of the peptide is 28.57 and comparable to those obtained for peptides with demonstrated membrane selective binding ability (41). Also, persistent and transient cation-π interactions between the side chains of lysine and phenylalanine might play a role in modulating the membrane selectivity. Thus, by preventing MSI-367 from assuming a transmembrane orientation, it must be possible to retard the formation of a pore structure in the membrane, and thereby prevent lysis of the target cell. It is worth mentioning here that non-pore forming short peptides would be less toxic to mammalian membranes and better candidates for cell targeting and pharmaceutical applications (1–6).

MSI-367 exhibits a broad-spectrum of antimicrobial and no hemolytic activities

Antimicrobial and hemolytic activities were performed as described earlier (37,41). The minimal inhibitory concentrations (MICs) of MSI-367 against *Escherichia coli*, *Staphylococcus aureus*, *Pseudomonas aeruginosa* and *Candida albicans* were determined from six independent experiments. MSI-367 exhibits activity against both Gram-positive and Gram-negative bacteria as well as *Candida albicans* as shown in Table 1. The reduced activity of MSI-367 against *Candida albicans* (higher MIC value as compared to those observed for bacteria) suggests either a difference in membrane composition or mechanism of membrane pemeabilization. At concentrations comparable to MIC values of bacteria, MSI-367 did not show any observable hemolytic activity. However, ~20% hemolysis was observed at 100 μg/mL of the peptide (Figure 1A). Hemolysis at high peptide concentrations

has been observed even for amyloid forming peptides that act on membranes by a different mechanism (49). Therefore, an understanding of the biophysical features of MSI-367 which displays cell selective activity would be useful for the future design of therapeutic peptides.

Bacterial outer-membrane permeabilization by MSI-367

The effective concentrations required to induce bacterial membrane permeabilization as opposed to the red blood cell membrane would reveal the difference in the mode of interaction of MSI-367 with biomembranes. We assessed the ability of MSI-367 to permeabilize the outer-membrane of Gram-negative *E. coli*, by measuring the enhancement in the fluorescent intensity of ANS, when ANS relocates into *E. coli* membrane interior (50). Being acidic at pH 7.4, ANS can penetrate into the hydrophobic membrane interior only when the membrane is substantially permeabilized. In a typical fluorimetry assay, *E. coli* cells harvested from mid-log phase culture were equilibrated with ANS (5.0 μM) for 5 min., and then treated with indicated concentrations of MSI-367 for 10 min. As shown in Figure 1B, MSI-367 induced the ANS relocation into *E. coli* membrane in a concentration dependent manner. It is imperative to note here that peptide induced osmotic lysis of *E. coli* cells did not occur during the experiment as cell density (OD_{600}) of the test sample before and after the addition of peptide remained comparable. Also, the outer-membrane permeabilization was observed at concentrations comparable to the MIC against *E. coli* cells. However, consideration of the cell densities used in these two assays point to the fact that much less peptide is required for outer-membrane permeabilization (see the Experimental Section). Since the peptide concentrations required for outer-membrane permeabilization and killing the bacteria (MIC) are different, peptide induced changes on membrane bilayers composed of different synthetic lipids and *E. coli* total lipids were studied.

Secondary structure of MSI-367 in a membrane environment is significantly different from that observed in solution

CD is a convenient technique to study the secondary structure of polypeptides in various media. Since MSI-367 exhibited distinct interactions with different membranes, we examined the effect of lipid vesicles on the structure of MSI-367 using CD experiments. Normalized CD spectra of MSI-367 in trifluoroethanol (TFE), PBS (pH = 7.4) and in the presence of SUVs prepared from POPC and *E. coli* total lipids are shown in Figure 2A. The CD spectrum of MSI-367 in aqueous buffer (trace 1) resembles the one with a largely unordered peptide structure. The positive maximum at ~218 nm and the negative minimum at ~200 nm might be the reminiscent of turn conformations (51). The spectrum of MSI-367 in neat TFE (trace 4) displays two negative minima at ~222 nm and ~208 nm suggesting the presence of a regularly folded α-helical conformation, as predicted. However, in the presence of POPC vesicles, the peptide shows a negative minimum at ~204 that suggests a random coil conformation. But, the low intensity of the band observed at ~204 (trace 2) argues against a 100 % random-coil conformation. Interestingly, the CD spectrum of MSI-367 in *E. coli* lipid vesicles exhibits a broad minimum ~224 nm (trace 3) suggestive of β-strand-like conformation. Even though the peptide-induced turbidity changes due to aggregation of vesicles observed during this experiment is in line with the β-strand conformation of peptide, caution must be exercised while interpreting the CD data as the turbidity of the sample might have distorted the observed profile. Nevertheless, the transition from a random-coil to an ordered secondary structure upon interaction with SDS micelles was confirmed from the proton NMR spectra of the peptide (Figure 2B).

MSI-367 induce positive curvature strain on DiPoPE lipid bilayers

Membrane bilayers composed of *E. coli* lipids, POPE and DiPoPE, are known to undergo transition from L_α to H_I and H_{II} phases above their phase transition temperatures (52). Cell

penetrating peptides have been shown to reduce the phase transition temperature of lipid vesicles (53). As shown in Figure 3, pure DiPoPE underwent the L_α to H_{II} phase transition at ~43°C. However, when MSI-367 was incorporated into DiPoPE at a P/L = 1/500 (0.2 mole % of MSI-367), the transition temperature increased by ~2°C (Figure 3). The transition temperature increased further when more amounts of MSI-367 were incorporated (Figure 4, 0.4 mole%). Thus, it appears that even at a P:L ratio of 1:500, MSI-367 induces positive curvature strain and encumbers the L_α to H_{II} phase transition of DiPoPE. This observation is consistent with ^{31}P-NMR data of POPE lipid bilayers containing MSI-367.

NMR experiments reveal MSI-367-induced structural changes in lipid bilayers

We used ^{31}P NMR to study the lipid headgroup conformation and ^{2}H NMR of deuterated-POPC (POPC-d_{31}) to measure the peptide-induced disorder in the hydrophobic part of the lipid bilayer. To understand how the transient lesions cause leakage, we examined the ^{2}H and ^{31}P NMR spectra of POPC, and ^{31}P NMR spectra of POPE, POPG and *E. coli* total lipid bilayers containing various amounts of MSI-367. de-Paked ^{2}H NMR spectra of pure POPC-d_{31} MLVs and POPC-d_{31} MLVs containing 3 and 5 mole % of MSI-367 are shown in Figure 4A. The well resolved quadrupolar splittings display the characteristic dynamic orders of the methylene (CD_2) units along the lipid acyl chain in the bilayer. As shown in Figure 4B, the difference in order parameters derived from the observed quadrupolar splittings are the highest for the CD_2 groups closer to the lipid head-group region and show a decreasing trend along the acyl chain towards a minimum for the other end of the chain, implying a strong localized effect at the water-bilayer interface.

To determine the peptide-induced structural changes in the water-bilayer interface region, ^{31}P NMR spectra were obtained from mechanically-aligned lipid bilayers. Figure 5 shows the ^{31}P NMR spectra of oriented POPC, POPG and POPE lipid bilayers incorporated with various amounts of MSI-367. ^{31}P NMR spectra of pure lipid bilayers display a narrow peak ~31 ppm (Figure 5, top traces), indicating that almost all lipids are aligned with the bilayer-normal parallel to the external magnetic field axis. However, ^{31}P NMR spectra of lipid bilayers incorporated with increasing amounts of MSI-367 show a concentration dependent shift towards the high-field region of the spectrum and broadening of the resonance ~31 ppm. Incorporation of 15 mole% of MSI-367 appears to disrupt the planar bilayer integrity substantially and promote non-planar structures (54,55). Thus, the peptide-induced membrane disruption seems to depend partly on the concentration regime, which determines the type of peptide-lipid complex at the water-bilayer interface.

Since phosphatidylethanolamine is the major lipid in *E. coli* membrane (56), understanding the interaction of MSI-367 with this lipid would provide insights into its mechanism of antibacterial action. ^{31}P NMR spectra of *E. coli* lipid bilayers incorporated with increasing amounts of MSI-367 are shown in Figure 6 and compared with that of bilayers containing pexiganan (MSI-78). Pexiganan, a well studied peptide antibiotic for diabetic foot ulcers, displays bactericidal activity (10). In the lower concentration regime (3 mole %), both pexiganan and MSI-367 seem to exert similar effects on *E. coli* lipid bilayers. However, distinctly different effects are seen at higher concentrations (5 mole% and above) of these peptides. While pexiganan appears to promote the formation of non-lamellar structures, MSI-367 clearly transforms the aligned planar bilayers into unaligned multilamellar structures. The differential activity displayed by these peptides might underscore the structural differences between the different types of lipid-peptide complexes formed. Since pexiganan is a bactericidal peptide, MSI-367 is likely to exert its antimicrobial activity by a different mechanism.

Enthalpy of MSI-367 interaction with lipids explains its bacterial selectivity

Since partitioning of hydrophobic residues into lipid bilayers usually results in a net negative enthalpy and partial insertion of peptides leads to a net positive enthalpy (57), we measured the enthalpy changes associated with the interactions of MSI-367 with POPC and *E. coli* lipid vesicles, to assess any lipid specific interactions. The heat capacity changes measured in μW from successive lipid into peptide titrations at 25 °C is presented in Figure 7 (top panel). The variation in enthalpy as a function of lipid/peptide ratio is given in Figure 7 (bottom panel). A qualitative analysis of Figure 7 reveals the two distinct modes of interaction of MSI-367 with zwitterionic POPC and acidic *E. coli* lipid vesicles. While the thermogram representing MSI-367 titrations with POPC (Figure 7A) suggests a two state binding to lipid vesicles, the interaction of the peptide with *E. coli* lipid vesicles leads to membrane fusion and aggregation (Figure 7B). It is imperative to note here that, visible small aggregates formed during the titrations settled down upon standing as a single large lump probably due to the exposure of hydrophobic moieties in the smaller aggregates. The two distinct modes of interaction of MSI-367 with zwitterionic POPC and anionic *E. coli* lipid vesicles clearly explain the bacterial cell selective activity of the peptide.

Membrane surface orientation of MSI-367 revealed by SFG experiments

Though ^{31}P and ^{2}H solid-state NMR experiments revealed the membrane-surface association of MSI-367, it would be valuable to determine the membrane orientation of the peptide at a lower peptide concentration. Therefore, the direct observation of monolayer surface specific interactions of the peptide observed in sum frequency generation (SFG) was utilized in this study. To get more insights on the membrane orientation of MSI-367, we used MSI-78 as a reference peptide. The SFG spectra of POPG bilayer in contact with MSI-367 or MSI-78 solution with a concentration of 0.8 μM are shown in Figure 8 for a comparison. Strong SFG signals and the fitted signal strength ratio of the *ppp* and *ssp* amide I spectra (χ_{ppp}/χ_{ssp}) obtained for MSI-78 (Figure 8A) indicate that MSI-78 strongly interacts with the POPG bilayer. The χ_{ppp}/χ_{ssp} ratio of 1.2 indicates the existence of more than one distinct orientation: some are inserted into the bilayer and others are oriented on the lipid bilayer surface (58) as shown in Figure 9. The membrane inserted orientation, or lining of the toroidal-pore surface, of MSI-78 is seen even for 0.4 μM concentration (data not shown). On the other hand, no discernable SFG signals are observed when the POPG bilayer is in contact with 0.8 μM MSI-367 solution (Figure 8B). Our data suggest that MSI-367 molecules are either not associated with the bilayer, or oriented on the lipid bilayer surface. When the MSI-367 concentration was increased to 1.2 μM, *ssp* signal was still not observed, and a weak SFG *ppp* signal (three or four times stronger than the noise) was detected (Figure 8C). Even when 1.2 μM solution of MSI-367 is in contact with the lipid bilayer, only the *ppp* signal and not the *ssp* signal is seen. The SFG signal intensity of 2.0 μM MSI-367 is, also, much weaker that of 0.8 μM MSI-78 (Figures 8A and 8D). Thus, our data clearly indicate that there is no insertion of MSI-367 into the hydrophobic core of the POPG bilayer. Both MSI-78 and MSI-367 have the same number of amino acids, helix propensity and 9 positively charged residues. Hence, it is likely that the high aliphatic index (93.18) of MSI-78 favors insertion into the lipid bilayer, while the low aliphatic index (28.57) of MSI-367 allows membrane interfacial localization of the peptide as suggested by NMR experiments.

The relationship between tilt angle (θ) and χ_{ppp}/χ_{ssp} is shown in Figure 9 in terms of different states of membrane bound peptides. The estimated *ppp/ssp* ratio obtained by curve-fitting for 0.8 μM MSI-78 is 1.2, and falls outside the curve simulated for a single helical orientation suggesting multiple helical orientation for the membrane bound peptide as shown in Figure 9 (right panel). On the other hand, the only *ppp* signal observed for 1.2 μM MSI-367 with a *ppp*/*ssp* signal strength ratio ~2, very different from that observed for

MSI-78, suggests that the alignment with POPG membrane of the peptide MSI-367 is very different from that observed for MSI-78. This significant difference between these two peptides can be attributed to the structural differences between them and explains the bacterial membrane selectivity of MSI-367.

Discussion

Design of highly potent and selective antimicrobial peptides is essential

Increasing bacterial resistance towards conventional antibiotic compounds is a major problem and therefore there is an urgent need for the development of compounds that could act via different types of mechanism is essential. Though the naturally-occurring antimicrobial peptides with a broad-spectrum of antibacterial activities are promising potential candidates to overcome this problem, large amount of peptide needed to kill bacteria is a major concern. To this end, several different strategies have been utilized to improve the potency and expanding the activity spectrum of antimicrobial peptides. Similarly, efforts have been directed towards reducing the cytotoxicity of cytolytic peptides. They include identification of the minimal fragment for antimicrobial activity (41,59), substitution of specific residues to reduce hemolytic activity (59,60), total or partial replacement by unusual and D-amino acids (14,61), use of retro- and retroenantiomeric analogs (62), cyclization and linearization of natural peptide antibiotics (37,63).

MSI-367 is a suitable antibacterial candidate with a very high bacterial selectivity

In this study, we have designed a synthetic AMP to evaluate the biophysical parameters required for selective activity against only bacteria and fungi, and not against human red blood cells. As predicted, MSI-367 shows activity against both bacteria and fungi (Table 1). It also permeabilizes the bacterial outer-membrane (Figure 1). In the observed range of MIC, the peptide does not exhibit any significant hemolytic activity, suggesting a non-lytic killing mechanism against bacteria (64). Although peptide-induced membrane permeabilization appears to be critical in eliciting the antimicrobial activity, a comparison of peptide concentrations and *E. coli* cell densities used for MIC determination (Table 1) and outer-membrane permeabilization (Figure 1) reveals a role for other factors in killing the bacterium. The lipid/protein ratio at the budding sites on *E. coli* membrane has been reported to be higher than that for the whole membrane. The protein depleted budding sites might turn into soft sites for peptide-induced outer-membrane permeabilization. This may explain the outer-membrane permeabilization observed at concentrations lower than MIC.

Membrane-water interface location of MSI-367 suppresses its hemolytic activity

Random-coil to α-helix conformational transitions upon binding to lipid membranes have been observed for several antimicrobial peptides (65). In the membrane mimicking solvent TFE, MSI-367 displays an α-helical conformation (Figure 2A, trace 4) which is consistent with the predicted amphipathic structure resulting from the segregation of hydrophilic and hydrophobic amino acids along the helical axis. Although the peptide has the intrinsic helical propensity, a qualitative analysis of the CD spectra of MSI-367 in the presence of POPC and *E. coli* lipid vesicles reveal only subtle variations in the conformation upon binding (Figure 2A, traces 2 and 3). However, a comparison of chemical shift values for amide-NH protons of MSI-367 in aqueous buffer (pH 6.0) and in the presence of 200 mM SDS-d_{25} micelles (Figure 2B) suggests substantial changes in the secondary structure of the peptide. When the peptide/SDS ratio was ~1:10, the peptide-SDS complex aggregated to form a precipitate. When more amounts of SDS were added, the solution became clear. It is important to note here that MSI-367 induced *E. coli* lipid aggregation during CD measurements suggesting interfacial association of the peptide. Similar behaviors have been

observed with AMPs such as indolicidin and tritrypticin. These peptides are rich in aromatic residues and bind only to the membrane interface (66,67).

^{2}H NMR experiments were used to measure the peptide-induced effect on the hydrophobic core of lipid bilayers. Addition of MSI-367 decreases the order parameter in a concentration dependent manner (Figure 4). The changes in the acyl chain order parameter suggest that the peptide binding induces disorder mainly in the interface region of POPC bilayers and maximum disorder is observed only near the glycerol backbone of the lipid. Negligible changes were observed in the order parameters of CD_2 groups near the terminal methyl group of the lipid that is consistent with the bilayer surface orientation of the peptide (50). DiPoPE and PE rich *E. coli* lipids have a tendency to form the inverted hexagonal phase with a negative curvature at higher temperatures due to their small head group size relative to the length of the acyl chain. Repression of Lα to H_{II} transition by membrane active peptides has been explained in terms of their surface bound states (68). Similarly, mitigation of Lα to H_{II} transition in DiPoPE liposomes by MSI-367 at low P:L ratio (Figure 3) observed in this study can be expected from the surface embedded peptide molecules. Thus, both ^{2}H-NMR and DSC studies point to a surface embedded as against a transmembrane orientation of membrane bound peptide. This prediction is also consistent with the observed changes in the ^{31}P NMR spectra of mechanically-aligned bilayers containing MSI-367 (Figure 5A–C). In addition, the peptide-induced lamellar to inverted hexagonal phase transition is clearly discernible in the case of *E. coli* lipid bilayers (Figure 6A) is in excellent agreement with the DSC data on synthetic DiPoPE lipid. Such transitions are not observed for a cell lytic antimicrobial peptide MSI-78 (Figure 6B). This unique behavior of MSI-367 is consistent with *E. coli* outer-membrane permeabilizing ability and non-hemolytic nature of the peptide at MIC.

The selective permeability of bacterial membrane can be expected from the peptide's ability to induce aggregation of *E. coli* lipids (observed during CD and ITC measurements) and SDS micelles at a P:L ratio of ~1:10 (observed during ^{1}H NMR measurements). Under these conditions, the antimicrobial peptide MSI-78 did not induce lipid aggregation consistent with its α-helix structure and toroidal-pore complex in lipid bilayers (68,69). ITC thermograms obtained from lipid into peptide titrations indicate a weak binding affinity for POPC vesicles (Figure 7A) and is in agreement with CD and ^{31}P-NMR spectra of MSI-367 in the presence of POPC. However, titrations of *E. coli* lipid vesicles into MSI-367 solution result in a thermogram indicative of both endothermic and exothermic processes (Figure 7B). While an exothermic process is expected from peptide-lipid interactions, the endothermic process can only arise from the loss of internal energy (54,57) of the system. Such a loss of internal energy could arise from the exposure of hydrophobic groups and/or transition from lipid bilayer to lamellar structures (54,57). The peptide-induced lamellar to inverted-hexagonal phase transition (Figure 6C) observed in *E. coli* lipid bilayers, is in agreement with the endo- and exothermic transitions seen in the thermogram (Figure 7B).

Antimicrobial peptides indolicidin and tritrypticin are rich in aromatic residues and bind to the lipid membrane interface (66,67). These peptides have been shown to induce lipid aggregation at certain P:L ratios. Since MSI-367 contains six aromatic residues and nine lysine residues, the lipids can effectively embrace the peptide at the lipid-water interface. Membrane-embedded peptide might then induce lipid aggregation as has been shown in the cases of indolicidin and tritrypticin (66,67). A comparison of SFG data (Figure 8) on POPG bound MSI-367 and MSI-78 clearly discloses the surface embedded orientation of non-hemolytic MSI-367 and the membrane insertion of hemolytic MSI-78 (70). Despite the fact that both MSI-367 and MSI-78 are cationic, and have intrinsic helix propensity and the required number of amino acids to form a transmembrane channel structure, it appears that the inability of MSI-367 to insert across the lipid bilayer makes it non-hemolytic. The

hemolytic activity observed at very high concentrations (>100 μg/mL) of MSI-367 might be similar to the toxicity observed with peptide amyloids where preformed peptide aggregates disrupt the cell membrane by an unknown mechanism. At higher concentrations of the peptide, binding of MSI-367 to negatively charged lipids and the disruption of the bilayer structure may involve the formation of inverted micelles (54,57). The proposed model (Figure 9) for antimicrobial activity of MSI-367 includes a non-lytic peptide-lipid complex in which the peptide lies on membrane surface in such a way that the lysine side chains are stretched out and the aromatic residues intercalated between the acyl chains at the water-bilayer interface. In this orientation, MSI-367 may induce a positive curvature strain which mitigates against the formation of H_{II} phase (Figure 3). This model also explains the peptide-induced changes in the phosphate headgroup conformation (Figure 5, 6) and the acyl chain disorder near the headgroups (Figure 4).

Conclusion

The non-lytic antimicrobial activity observed against *E. coli* at ~1.6 μM concentration could be explained in terms of the moderate aliphatic index and the 9 cationic residues of MSI-367 that confer membrane-water interfacial localization of the peptide as charged molecules cannot cross the lipid bilayer by passive diffusion because of the high Born energy penalty encountered in a medium of low dielectricity (71). ^{31}P-NMR data of *E. coli* lipid bilayers clearly indicate the formation of unaligned multilamellar lipid structures and suggest that the toroidal-type pore mechanism is unlikely. ^{2}H NMR, DSC and SFG studies confirm the lipid bilayer interfacial localization of MSI-367. Taken together our results suggest that limiting the action of antimicrobial peptides to membrane-water interface bears the advantage for improving the therapeutic potential of AMPs as the cell-lytic peptides are not the desirable candidates because of their toxicity.

Acknowledgments

This research was supported by the research funds from NIH (AI054515, GM084018 and RR023597 to A.R and GM081655-01A2 to ZC), CRIF-NSF funding for the NMR spectrometer, and the Office of Naval Research (N00014-08-1-1211 for ZC). We thank Dr. Tan for help with fluorescence experiments and Dr. Vivekanandan for recording proton NMR spectra of MSI-367. We thank the biomolecular 900 MHz NMR facility at East Lansing, MI.

Abbreviations

CSA	chemical shift anisotropy
CD	circular dichroism
DiPoPE	1,2-dipalmitoleoyl-sn-glycero-3-phosphotydylethanolamine
DSC	differential scanning calorimetry
H_I	normal hexagonal phase
H_{II}	inverted hexagonal phase
ITC	isothermal titration calorimetry
L_α	fluid lamellar phase
MIC	minimum inhibitory concentration
MLVs	multilamellar vesicles
NMR	nuclear magnetic resonance

POPC	1-palmitoyl-2-oleoyl-sn-glycero-3-phosphatidylcholine
POPC-d_{31}	1-d_{31}-palmitoyl-2-oleoyl-sn-glycero-3-phosphatidylcholine
POPG	1-palmitoyl-2-oleoyl-sn-glycero-3-phosphatidylglycerol
POPE	1-palmitoyl-2-oleoyl-sn-glycero-3-phosphatidylethanolamine
SUVs	small unilamellar vesicles

References

1. Giuliani A, Pirri G, Nicoletto SF. Antimicrobial peptides: an overview of a promising class of therapeutics. Centr Eur J Biol. 2007; 2:1–33.
2. Zasloff M. Antimicrobial peptides of multicellular organisms. Nature. 2002; 415:389–395. [PubMed: 11807545]
3. Shai Y, Makovitzky A, Avrahami D. Host defense peptides and lipopeptides: Modes of action and potential candidates for the treatment of bacterial and fungal infections. Curr Protein Pept Sci. 2006; 7:479–486. [PubMed: 17168781]
4. Hancock REW, Sahl H-G. Antimicrobial and host-defense peptides as new anti-infective therapeutic strategies. Nature Biotechnol. 2006; 24:1551–1557. [PubMed: 17160061]
5. Diamond G, Beckloff N, Weinberg A, Kisich KO. The roles of antimicrobial peptides in innate host defense. Curr Pharm Des. 2009; 15:2377–2392. [PubMed: 19601838]
6. Dhople V, Krukemeyer A, Ramamoorthy A. The human beta-defensin-3, an antibacterial peptide with multiple biological functions. Biochim Biophys Acta. 2006; 1758:1499–1512. [PubMed: 16978580]
7. Bhattacharjya S, Ramamoorthy A. Multifunctional host defense peptides: functional and mechanistic insights from NMR structures of potent antimicrobial peptides. FEBS J. 2009; 276:6465–6473. [PubMed: 19817858]
8. Epand RF, Maloy L, Ramamoorthy A, Epand RM. Amphipathic helical cationic antimicrobial peptides promote rapid formation of crystalline states in the presence of phosphatidylglycerol: lipid clustering in anionic membranes. Biophys J. 2010; 98:2564–2573. [PubMed: 20513400]
9. Matsuzaki K, Sugishita K, Fujii N, Miyajima K. Translocation of a channel-forming antimicrobial peptide, magainin 2, across lipid bilayers by forming a pore. Biochemistry. 1995; 34:6521–6526. [PubMed: 7538786]
10. Ge G, MacDonald DL, Holroyd KJ, Thornsberry C, Wexler H, Zasloff M. *In vitro* antibacterial properties of pexiganan, an analog of magainin. Antimicrob Agents Chemother. 1999; 43:782–788. [PubMed: 10103181]
11. Zhang L, Falla TJ. Host defense peptides for use as potential therapeutics. Clin Dermatol. 2009; 27:485–494. [PubMed: 19695481]
12. Liu Z, Young AW, Hu P, Rice AJ, Zhou C, Zhang Y, Kallenbach NR. Turning the membrane selectivity of antimicrobial peptides by using multivalent design. ChemBioChem. 2007; 8:2063–2065. [PubMed: 17924379]
13. Glukhov E, Stark M, Burrows LL, Deber CM. Basis for Selectivity of Cationic Antimicrobial Peptides for Bacterial Versus Mammalian Membranes. J Biol Chem. 2005; 280:33960–33967. [PubMed: 16043484]
14. Zhu WL, Nan YH, Hahm KS, Shin SY. Cell selectivity of an antimicrobial peptide melittin diastereomer with D-amino acid in the leucine zipper sequence. J Biochem Mol Biol. 2007; 40:1090–1094. [PubMed: 18047808]
15. Lu J-X, Blazyk J, Lorigan GA. Exploring membrane selectivity of the antimicrobial peptide KIGAKI using solid-state NMR spectroscopy. Biochim Biophys Acta (Biomembranes). 2006; 1758:1303–1313.
16. Eckert R, Qi F, Yarbrough DK, He J, Anderson MH, Wenyuan S. Adding selectivity to antimicrobial peptides: Rational design of a multidomain peptide against *Pseudomonas spp*. Antimicrob Agents and Chemother. 2006; 50:1480–1488. [PubMed: 16569868]

17. Gottler L, Ramamoorthy A. Membrane Orientation, Mechanism, and Function of Pexiganan - A Highly Potent Antimicrobial Peptide Designed From Magainin. Biochim Biophys Acta. 2009; 1788:1680–1686. [PubMed: 19010301]

18. Marsh ENG, Buer BC, Ramamoorthy A. Fluorine-a new element in the design of membrane-active peptides. Molec BioSyst. 2009; 5:1143–1147. [PubMed: 19756303]

19. Bringezu F, Wen S, Dante S, Hauss T, Majerowicz M, Waring A. The insertion of the antimicrobial peptide dicynthaurin monomer in model membranes: Thermodynamics and structural characterization. Biochemistry. 2007; 46:5678–5686. [PubMed: 17451228]

20. Pistolesi S, Pogni R, Feix JB. Membrane insertion and bilayer perturbation by antimicrobial peptide CM15. Biophys J. 2007; 93:1651–1660. [PubMed: 17496013]

21. Lee TH, Hall KN, Swann MJ, Popplewell JF, Unabia S, Park Y, Hahm KS, Aguilar MI. The membrane insertion of helical antimicrobial peptides from the N-terminus of Helicobacter pylori ribosomal protein L1. Biochim Biphys Acta. 2010; 1798:544–557.

22. Ramamoorthy A, Lee DK, Narasimhaswamy T, Nanga RPR. Cholesterol reduces pardaxin's dynamics-a barrel-stave mechanism of membrane disruption investigated by solid-state NMR. Biochim Biophys Acta. 2010; 1798:223–227. [PubMed: 19716800]

23. Ramamoorthy A. Beyond NMR spectra of antimicrobial peptides: Dynamical images at atomic resolution and functional insights. Solid State Nucl Magn Res. 2009; 35:201–207.

24. Serrano GN, Zhanel GG, Schweizer F. Antibacterial Activity of Ultrashort Cationic Lipo-beta-Peptides. Antimicrob Agents Chemother. 2009; 53:2215–2217. [PubMed: 19237652]

25. Gehman JD, Luc F, Hall K, Lee TH, Boland MP, Pukala TL, Bowie JH, Aguilar M, Separovic F. Effect of antimicrobial peptides from Australian tree frogs on anionic phospholipid membranes. Biochemistry. 2008; 47:8557–8565. [PubMed: 18652483] Strøm MB, Rekdal Ø, Svendsen JS. Antimicrobial activity of short arginine- and tryptophan-rich peptides. J Petide Sci. 2002; 8:431–437.

26. Blondelle SE, Takahashi E, Dinh KT, Houghten R. The antimicrobial activity of hexapeptides derived from synthetic combinatorial libraries. J Applied Microbiol. 1995; 78:39–46.

27. Shamova O, Orlov D, Stegemann C, Czihal P, Hoffmann R, Brogden K, Kolodkin N, Sakuta G, Tossi A, Sahl HG, Kokryakov V, Lehrer RI. A novel proline-rich antimicrobial peptide from goat leukocytes. Int J Pep Prot Res. 2009; 15:108–119.

28. Chen C, Pan F, Zhang S, Hu J, Cao M, Wang J, Xu H, Zhao X, Lu JR. Antibacterial Activities of Short Designer Peptides: a Link between Propensity for Nanostructuring and Capacity for Membrane Destabilization. Biomacromol. 2010; 11:402–411.

29. Dartois V, Sanchez-Quesada J, Cabezas E, Chi E, Dubbelde C, Dunn C, Granja J, Gritzen C, Weinberger D, Ghadiri MR, Thomas R, Parr TR Jr. Systemic antibacterial activity of novel synthetic cyclic peptides. Antimicrob Agents and Chemother. 2005; 49:3302–3310. [PubMed: 16048940]

30. Fernandez-Lopez S, Kim H-S, Choi EC, Delgado M, Granja JR, Khasanov A, Kraehenbuehl K, Long G, Weinberger DA, Wilcoxen KM, Ghadiri MR. Antibacterial agents based on the cyclic D,L-alpha-peptide architecture. Nature. 2001; 412:452–455. [PubMed: 11473322]

31. Ganz T. Defensins: Antimicrobial peptides of innate immunity. Nat Rev Immunol. 2003; 3:710–720. [PubMed: 12949495]

32. Abuja PM, Zenz A, Trai M, Craik DL, Lohner K. The cyclic antimicrobial peptide RTD-1 induces stabilized lipid-peptide domains more efficiently than its open-chain analogue. FEBS Lett. 2004; 566:301–306. [PubMed: 15147913]

33. Thennarasu S, Lee DK, Poon A, Kawulka KE, Vederas JC, Ramamoorthy A. Membrane permeabilization, orientation, and antimicrobial mechanism of subtilosin A. Chem Phys Lipids. 2005; 137:38–51. [PubMed: 16095584]

34. Papo N, Shai Y. New lytic peptides based on the D,L-amphipathic helix motif preferentially kill tumor cells compared to normal cells. Biochemistry. 2003; 42:9346–9354. [PubMed: 12899621]

35. Vad BS, Bertelsen K, Johansen CH, Pedersen JM, Skrydstrup T, Nielsen NC, Otzen DE. Pardaxin Permeabilizes Vesicles More Efficiently by Pore Formation than by Disruption. Biophys J. 2010; 98:576–585. [PubMed: 20159154]

36. Asthana N, Yadavand SP, Ghosh JK. Dissection of antibacterial and toxic activity of melittin - A leucine zipper motif plays a crucial role in determining its hemolytic activity but not antibacterial activity. J Biol Chem. 2004; 279:55042–55050. [PubMed: 15475354]
37. Ramamoorthy A, Thennarasu S, Tan A, Gottipati K, Sreekumar S, Heyl DL, An FY, Shelburne CE. Deletion of all cysteines in tachyplesin I abolishes hemolytic activity and retains antimicrobial activity and lipopolysaccharide selective binding. Biochemistry. 2006; 45:6529–6540. [PubMed: 16700563]
38. Gottler LM, de la Salud Bea R, Shelburne CE, Ramamoorthy A, Marsh EN. Using Flourous Amino Acids to Probe the Effects of Changing Hydrophobicity on the Physical and Biological Properties of the Beta-Hairpin Antimicrobial Peptide Protegrin-1. Biochemistry. 2008; 47:9243–9250. [PubMed: 18693751]
39. Chen Y, Mant CT, Farmer SW, Hancock REW, Vasil ML, Hodges RS. Rational design of alpha-helical antimicrobial peptides with enhanced activities and specificity/therapeutic index. J Biol Chem. 2005; 280:12316–12329. [PubMed: 15677462]
40. Scott RW, DeGrado WF, Tew GN. *de novo* designed synthetic mimics of antimicrobial peptides. Curr Opin Biotech. 2008; 19:620–627. [PubMed: 18996193]
41. Thennarasu S, Tan A, Penumatchu R, Shelburne CE, Heyl DL, Ramamoorthy A. Antimicrobial and membrane disrupting activities of a peptide derived from the human cathelicidin antimicrobial peptide LL37. Biophys J. 2010; 98:248–257. [PubMed: 20338846]
42. Hallock KJ, Henzler-Wildman K, Lee DK, Ramamoorthy A. An innovative procedure using a sublimable solid to align lipid bilayers for solid-state NMR studies. Biophys J. 2002; 82:2499–2503. [PubMed: 11964237]
43. Wang J, Chen C, Buck SM, Chen Z. Molecular chemical structure on poly(methyl methacrylate) (PMMA) surface studied by sum frequency generation (SFG) vibrational spectroscopy. J Phys Chem B. 2001; 105:12118–12125.
44. Nguyen KT, Le Clair SV, Ye SJ, Chen Z. Molecular interactions between magainin 2 and model membranes *in situ*. J Phys Chem B. 2009; 113:12358–12363. [PubMed: 19728722]
45. Castano S, Cornut I, Büttner K, Dasseux JL, Dufourcq J. The amphipathic helix concept: length effects on ideally amphipathic LiKj(i=2j) peptides to acquire optimal hemolytic activity. Biochim Biophys Acta. 1416:161–175. [PubMed: 9889358]
46. Kyte J, Doolittle RF. A simple method for displaying the hydropathic character of a protein. J Mol Biol. 1982; 157:105–132. [PubMed: 7108955]
47. Ikai AJ. Thermostability and aliphatic index of globular-proteins. J Biochem. 1980; 88:1895–1898. [PubMed: 7462208]
48. Garnier J, Gibrat JF, Robson B. GOR method for predicting protein secondary structure from amino acid sequence. Comp Meth Macromol Seq Anal. 1996; 266:540–553.
49. Yoshiike Y, Kayed R, Milton S, Takashima A, Glabe C. Pore-forming proteins share structural and functional homology with amyloid oligomers. NeuroMol Med. 2007; 9:270–275.
50. Thennarasu S, Lee D-K, Tan A, Prasad Kari U, Ramamoorthy A. Antimicrobial activity and membrane selective interactions of a synthetic lipopeptide MSI-843. Biochim Biophys Acta. 2005; 1711:49–58. [PubMed: 15904663]
51. Thennarasu S, Nagaraj R. Solution conformations of peptides representing the sequence of the toxin pardaxin and analogues in trifluoroethanol-water mixtures: Analysis of CD spectra. Biopolymers. 1997; 41:635–645. [PubMed: 9108731]
52. Siegel DP, Epand RM. Effect of influenza hemagglutinin fusion peptide on lamellar/inverted phase transitions in dipalmitoleoylphosphatidylethanolamine: implications for membrane fusion mechanisms. Biochim Biophys Acta. 2000; 1468:87–98. [PubMed: 11018654]
53. Alves ID, Goasdoué N, Correia I, Aubry S, Galanth C, Sagan S, Lavielle S, Chassaing G. Membrane interaction and perturbation mechanisms induced by two cationic cell penetrating peptides with distinct charge distribution. Biochim Biophys Acta. 2008; 1780:948–959. [PubMed: 18498774]
54. Reshetnyak YK, Andreev OA, Segala M, Markin VS, Engelman DM. Energetics of peptide (pHLIP) binding to and folding across a lipid bilayer membrane. Proc Natl Acad Sci (USA). 2008; 105:15340–15345. [PubMed: 18829441]

55. Wi S, Kim C. Pore structure, thinning effect, and lateral diffusive dynamics of oriented lipid membranes interacting with antimicrobial peptide protegrin-1: ^{31}P and ^{2}H solid-state NMR study. J Phys Chem B. 2008; 112:11402–11414. [PubMed: 18700738]
56. Hallock KJ, Lee DK, Ramamoorthy A. MSI-78, an analogue of the magainin antimicrobial peptides, disrupts lipid bilayer structure via positive curvature strain. Biophys J. 2003; 84:3052–3060. [PubMed: 12719236]
57. Morein S, Andersson A, Rilfors L, Lindblom G. Wild-type Escherichia coli cells regulate the membrane lipid composition in a “window” between gel and non-lamellar structures. J Biol Chem. 1996; 271:6801–6809. [PubMed: 8636103]
58. Nguyen KT, Le Clair SV, Ye S, Chen Z. Orientation Determination of Protein Helical Secondary Structures Using Linear and Nonlinear Vibrational Spectroscopy. J Phys Chem B. 2009; 113:12169–12180. [PubMed: 19650636]
59. Lee KH, Hong SY, Oh JE, Kwon MY, Yoon JH, Lee JH, Lee BL, Moon HM. Identification and characterization of the antimicrobial peptide corresponding to C-terminal beta-sheet domain of tenecin 1, an antibacterial protein of larvae of Tenebrio molitor. Biochem J. 1998; 334:99–105. [PubMed: 9693108]
60. Andrushchenko VV, Aarabi MH, Nguyen LT, Prenner EJ, Vogel HJ. Thermodynamics of the interactions of tryptophan-rich cathelicidin antimicrobial peptides with model and natural membranes. Biochim Biophys Acta. 2008; 1778:1004–1014. [PubMed: 18222168]
61. Park S-C, Kim M-H, Hossain MA, Shin SY, Kim Y, Stella L, Wade JD, Park Y, Hahm K-S. Amphipathic alpha-helical peptide, HP (2–20), and its analogues derived from Helicobacter pylori: Pore formation mechanism in various lipid compositions. Biochim Biophys Acta. 2008; 1778:229–241. [PubMed: 17961502]
62. Rodríguez A, Villegas E, Satake H, Possani LD, Corzo G. Amino acid substitutions in an alpha-helical antimicrobial arachnid peptide affect its chemical properties and biological activity towards pathogenic bacteria but improves its therapeutic index. Amino Acids. 2009 (in Press).
63. Pouny Y, Shai Y. Interaction of D-amino-acid incorporated analogs of paradoxin with membranes. Biochemistry. 1992; 31:9482–9490. [PubMed: 1390731]
64. Cheng JTJ, Hale JD, Elliot M, Hancock REW, Straus SK. Effect of Membrane Composition on Antimicrobial Peptides Aurein 2.2 and 2.3 From Australian Southern Bell Frogs. Biophys J. 96:552–565. [PubMed: 19167304] Epand RM, Vogel HJ. Diversity of antimicrobial peptides and their mechanisms of action. Biochim Biophys Acta. 1999; 1462:11–28. [PubMed: 10590300]
65. Oren Z, Shai Y. Cyclization of a cytolytic amphipathic alpha-helical peptide and its diastereomer: Effect on structure, interaction with model membranes, and biological function. Biochemistry. 2000; 39:6103–6114. [PubMed: 10821683]
66. Henriques ST, Castanho MARB. Consequences of nonlytic membrane perturbation to the translocation of the cell penetrating peptide pep-1 in lipidic vesicles. Biochemistry. 2004; 43:9716–9724. [PubMed: 15274626]
67. Lequin O, Ladram A, Chabbert L, Bruston F, Convert O, Vanhoye D, Chassaing G, Nicolas P, Amiche M. Dermaseptin S9, an alpha-helical antimicrobial peptide with a hydrophobic core and cationic termini. Biochemistry. 2006; 45:468–480. [PubMed: 16401077]
68. Ramamoorthy A, Thennarasu S, Lee DK, Tan A, Maloy L. Solid-state NMR investigation of the membrane-disrupting mechanism of antimicrobial peptides MSI-78 and MSI-594 derived from magainin 2 and melittin. Biophys J. 2006; 91:206–216. [PubMed: 16603496]
69. Rozek A, Friedrich CL, Hancock REW. Structure of the bovine antimicrobial peptide indolicidin bound to dodecylphosphocholine and sodium dodecyl sulfate micelles. Biochemistry. 2000; 39:15765–15774. [PubMed: 11123901]
70. Schibli DJ, Nguyen LT, Kernaghan SD, Rekdal Ø, Vogel HJ. Structure-function analysis of tritrpticin analogs: Potential relationships between antimicrobial activities, model membrane interactions, and their micelle-bound NMR structures. Biophys J. 2006; 91:4413–4426. [PubMed: 16997878]
71. Bechinger B. Towards membrane protein design: pH-sensitive topology of histidine-containing polypeptides. J Mol Biol. 1996; 263:768–775. [PubMed: 8947574]

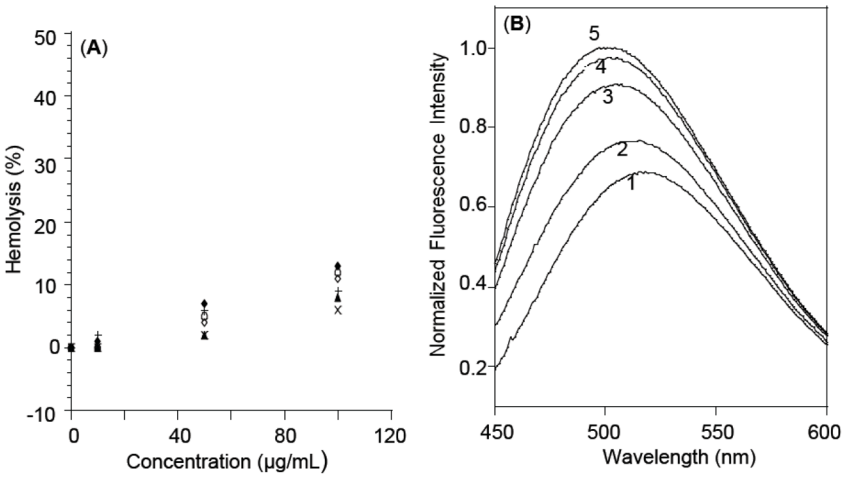

Figure 1.

(A) Hemolysis profile of MSI-367 in six independent experiments at indicated concentrations (μg/mL). Maximum lysis (100%) was observed with 2% Triton 100. (B) MSI-367 induced ANS uptake into *E. coli* membrane. Fluorescence spectrum of ANS equilibrated with *E. coli* cells (1), and in the presence of 0.67 μM (2), 1.33 μM (3), 2.0 μM (4) and 2.67 μM (5) quantities of MSI-367. The *E. coli* cell density, as measured by the $OD_{600,}$ was 1.20. The blue shift in the fluorescence emission maximum indicates the extent of penetration of ANS into E. *coli* membrane as a function of peptide concentration.

Figure 2A

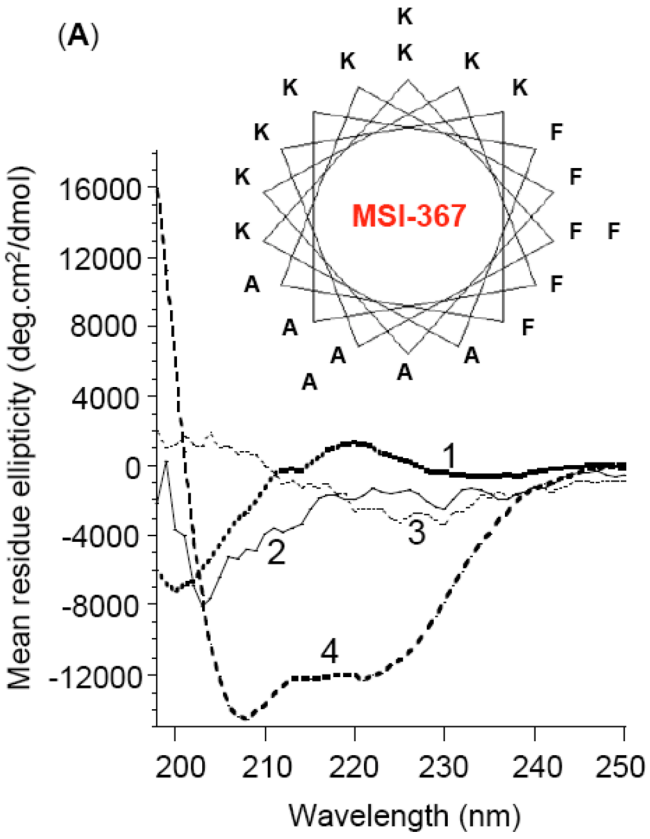

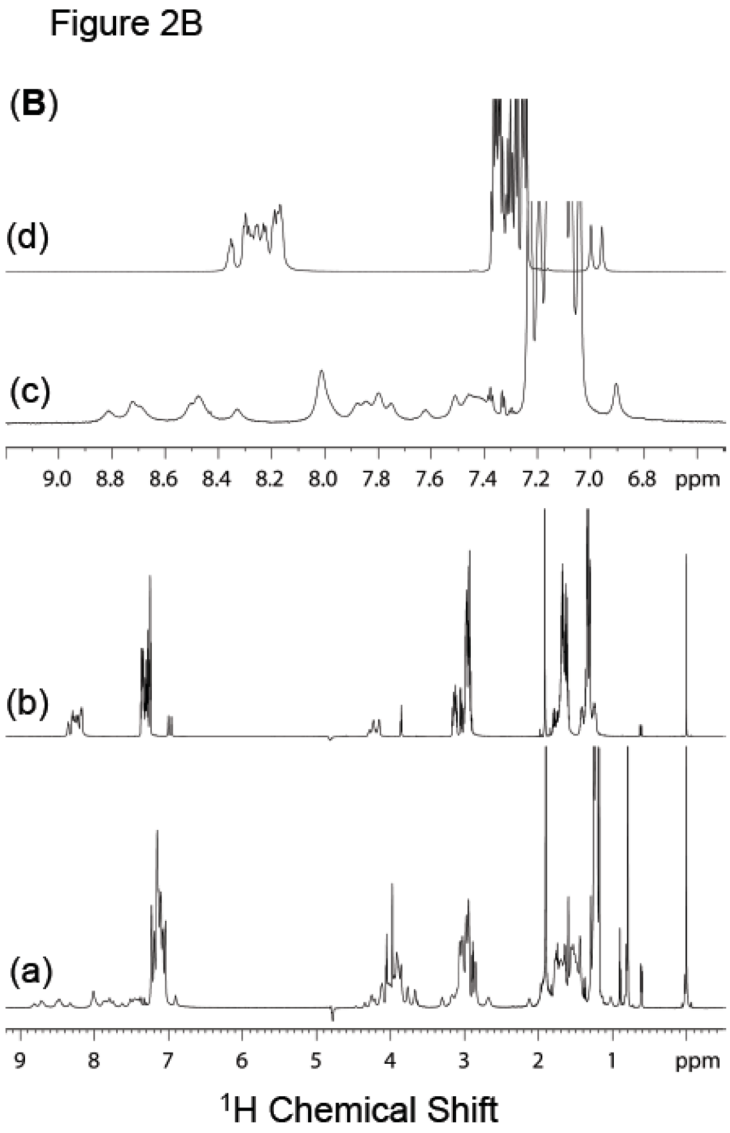

Figure 2.

(A) Helix wheel representation of MSI-367 and CD spectra of MSI-367 in different media: phosphate buffered saline pH 7.4 (1), SUVs of POPC (2), SUVs of E. coli total lipids (3), and TFE (4). Peptide concentration was 30 μM. The concentration of POPC was 550 μM, and that of *E. coli* lipids was 840 μM. When all the residues are assumed to be part of the helix, the polar angle subtended by the helix is 154°. (B) ^{1}H-NMR spectra of MSI-367: 2.53 mM peptide in 20 mM sodium phosphate buffer (pH 6.0) (traces (b) and (d)) obtained from a 900 MHz Bruker spectrometer (East Lansing, MI); 1.5 mM peptide and 180 mM SDS-d23 in 10 mM sodium phosphate buffer (pH 6.0) (traces (a) and (c)).

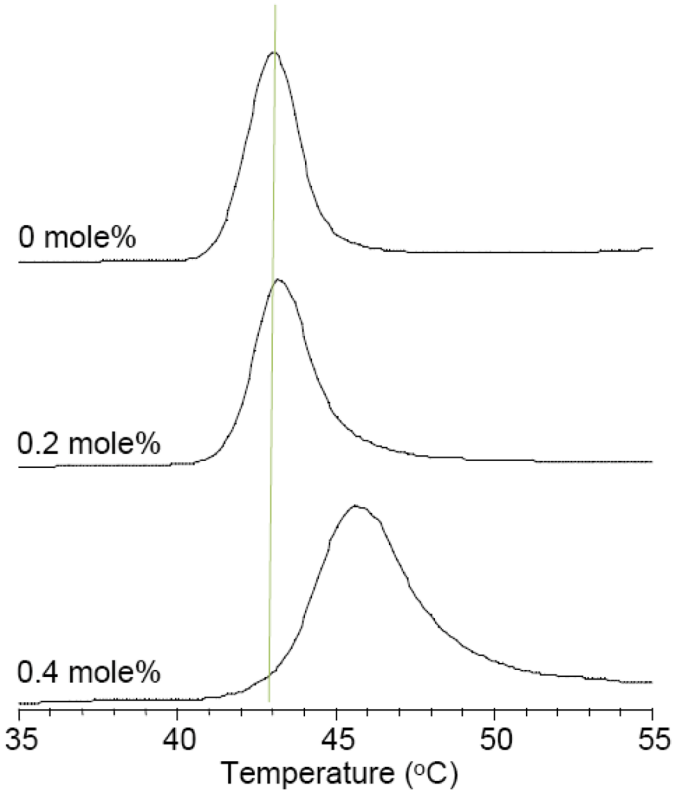

Figure 3.
DSC thermograms of DiPoPE incorporated with different concentrations of MSI-367. The heating scan rate was 1 °C/min. The vertical dotted line shows the phase transition temperature (T_m=43 °C) of pure DiPoPE. The phase transition thermograms of DiPoPE containing 0.2 and 0.4 mole% of peptide are also shown.

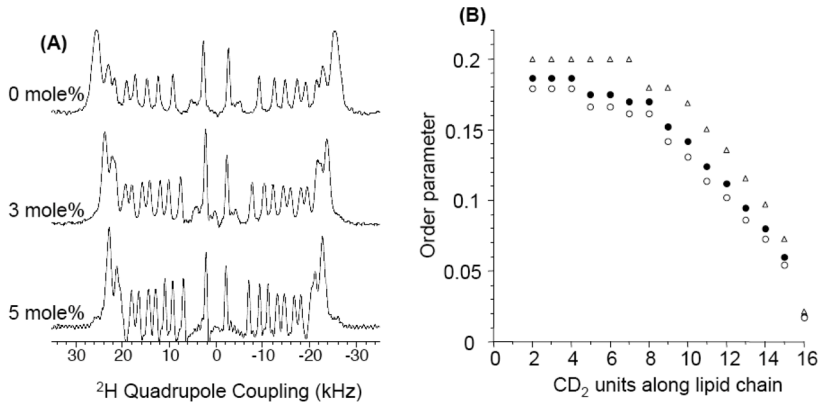

Figure 4.

(A) de-Paked ^{2}H quadrupole coupling spectra of POPC-d_{31} MLVs and POPC-d_{31} MLVs incorporated with 3 and 5 mole% of MSI-367. (B) Plot of order parameter versus lipid acyl chain carbon number: POPC-d_{31} (empty triangles), POPC-d_{31}/3 mol%MSI-367 (filled circles), POPC-d_{31}/5 mol%MSI-367 (empty circles).

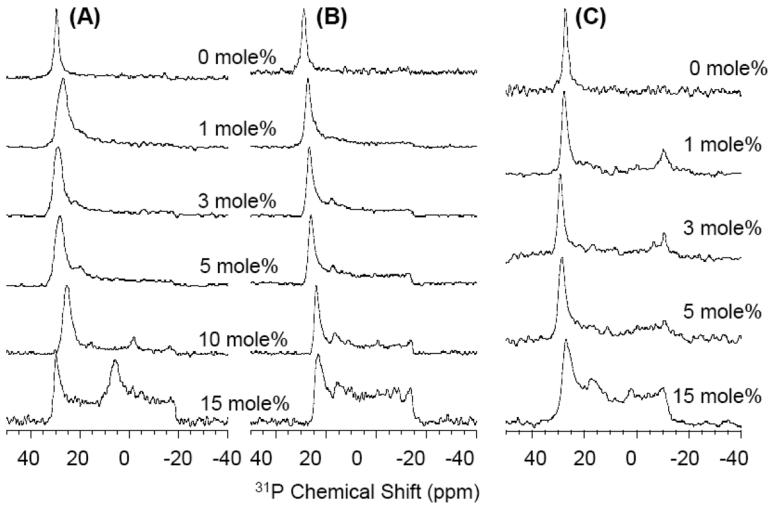

Figure 5.

^{31}P chemical shift spectra of aligned POPC (A), POPE (B) and POPG (C) lipid bilayers in the presence and absence of MSI-367. The peptide concentrations are indicated in the figure. Each spectrum was obtained from 4 mg lipids and required 100–1000 transients.

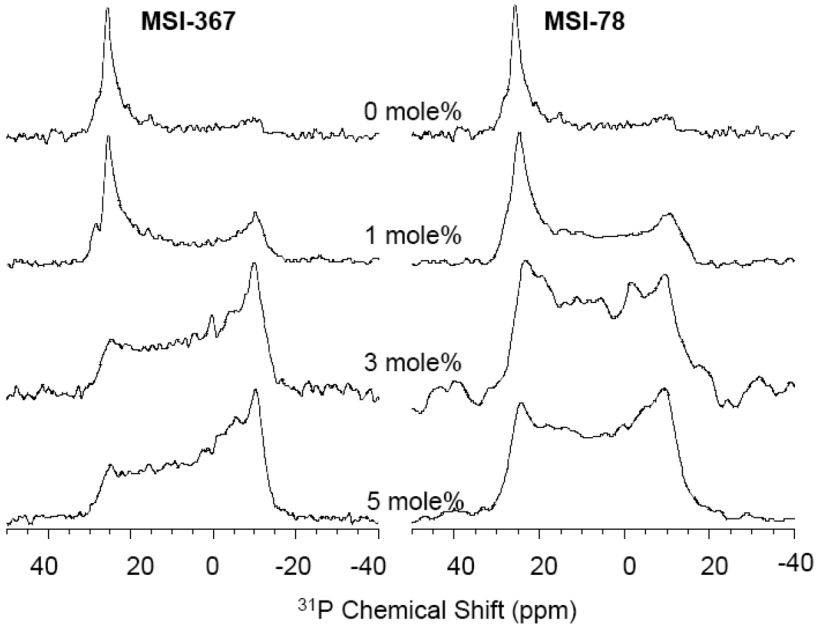

Figure 6.
^{31}P chemical shift spectra of aligned *E. coli* lipid bilayers in the presence and absence of MSI-367 (A) and MSI-78 (B). The peptide concentrations are indicated in the figure. Each spectrum was obtained from 4 mg lipids and required 100–1000 transients.

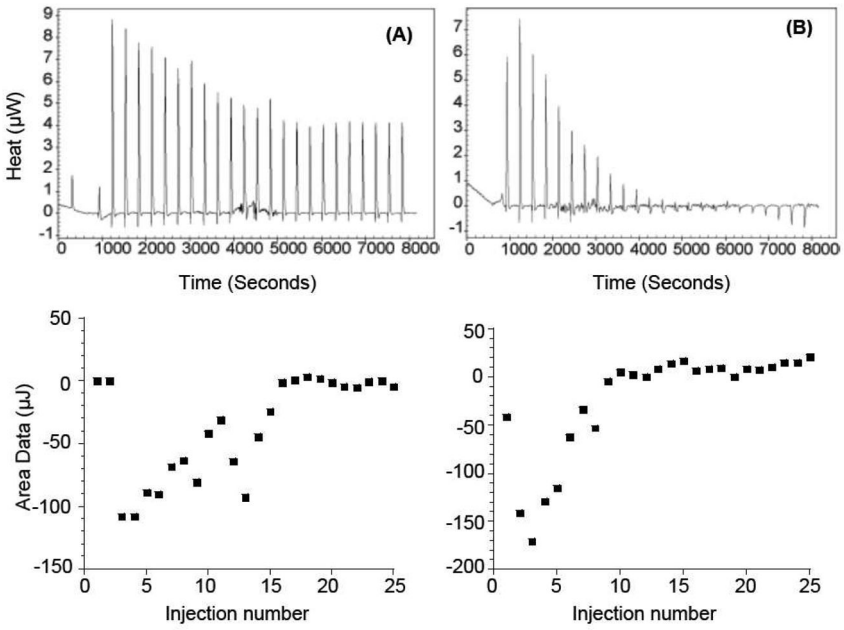

Figure 7.

Titration calorimetry thermograms of POPC (A) and *E. coli* (B) lipid into peptide titrations. Aliquots of a 10 μL lipid solution (~20 mM) were added to the peptide solution (5 μM) in the reaction cell (V = 1.0 mL). Top panel shows the calorimeter trace. The enthalpy of reaction, which is calculated by integration of the calorimeter traces, is given in bottom panel.

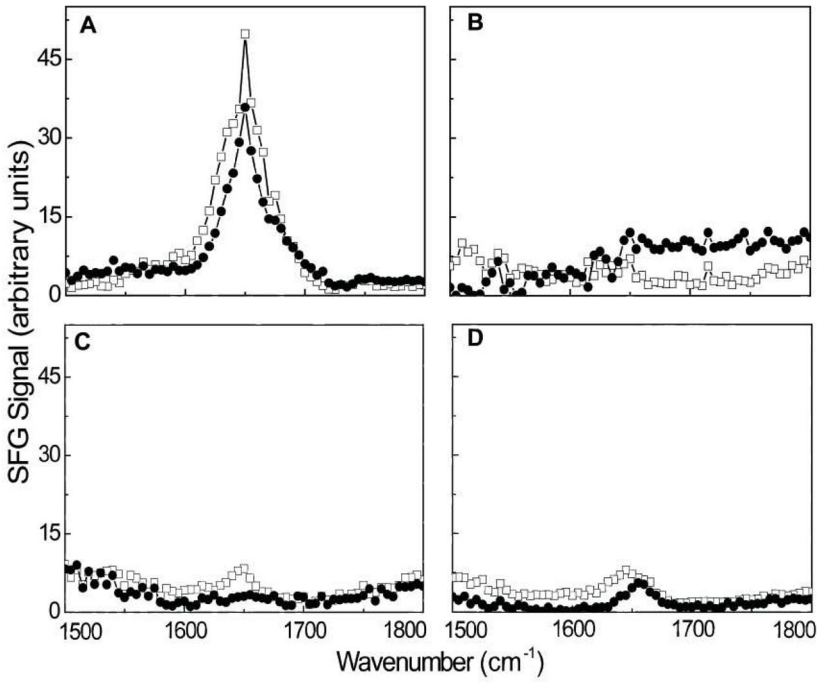

Figure 8.

SFG-Vibrational spectra: Amide I signals obtained from the single POPG bilayer in contact with 0.8 μM MSI-78 (A), and 0.8 μM (B), 1.2 μM (C) and 2.0 μM (D) MSI-367 solutions. Open squares: *ppp* spectra; filled squares: *ssp* spectra. While there is no signal observed from 0.8 μM MSI-367, a low-intensity *ppp* signal was observed for 1.2 μM concentration of the peptide.

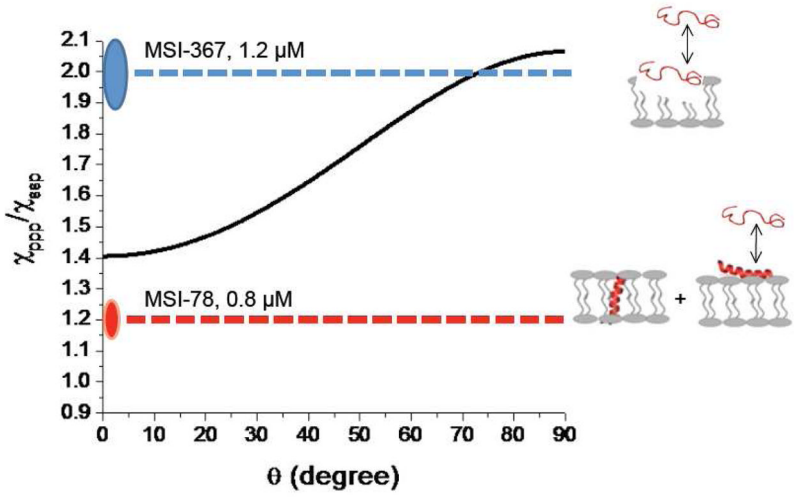

Figure 9.

The solid line represents the relationship between the SFG *ppp*/*ssp* signal strength ratio and the tilt angle (θ) of a helical peptide by assuming an identical orientation relative to the lipid bilayer-normal. Experimentally measured data points are shown for 0.8 μM MSI-78 and 1.2 μM MSI-367.

Table 1

Determination of minimum inhibitory concentration of MSI-367 against microbes.

Microorganism	Expt. 1	Expt. 2	Expt. 3	Expt. 4	Expt. 5	Expt. 6	MIC (μg/mL)
S. aureus	4	4	4	4	4	8	4 (1.6)*
P. aeruginosa	8	8	4	4	8	8	8 (2.8)
E. coli	4	4	2	4	4	8	4 (1.6)
C. albicans	64	64	64	128	64	64	64 (25.8)

* Numbers given in parentheses are the MIC values in μM concentration.